Supporting Information for "Designing a radiative antidote to CO_2"

Jacob T. Seeley[1], Nicholas J. Lutsko[2], David W. Keith[3]

[1]Harvard University Center for the Environment

[2]Scripps Institution of Oceanography

[3]John A. Paulson School of Engineering and Applied Sciences (SEAS), Harvard Kennedy School, Harvard University

Contents of this file

1. Supplementary text: Numerical Modeling
2. Figures S1 to S3

Numerical Modelling We simulated radiative-convective equilibrium with the cloud-resolving model Das Atmospharische Modell (DAM) (Romps, 2008). DAM's dynamical core is fully-compressible and nonhydrostatic, and subgrid-scale turbulence is handled by "implicit large-eddy simulation" (Margolin et al., 2006). Turbulent fluxes of sensible and latent heat from the surface were modeled with a standard bulk aerodynamic formula with drag coefficient 1.5×10^{-3} and a fixed wind surface speed of 5 m/s. Domain-mean

---

Corresponding author: Jacob T. Seeley, Harvard University Center for the Environment, Cambridge, MA. (jacob.t.seeley@gmail.com)

horizontal winds at each level were nudged to zero on a timescale of 1 hour. The square domain was doubly-periodic with side length 96 km and horizontal resolution $\Delta x = \Delta y =$ 2 km. The stretched vertical grid had 64 levels, with a model top at $\simeq$ 32 km, and with $\Delta z \simeq 100$ m resolution in the boundary layer, $\Delta z \simeq 500$ m in the free troposphere, and $\Delta z \simeq 1$ km in the stratosphere.

DAM typically uses the Lin-Lord-Krueger bulk microphysics scheme (Lin et al., 1983; Lord et al., 1984; Krueger et al., 1995). However, for this study we use a variant of the minimally-complex cloud microphysics parameterization described in (Seeley et al., 2019). In this simplified scheme, there is no ice phase (i.e., water is modeled as a two-phase substance, with latent heat associated with phase change between vapor and liquid only). Accordingly, only three bulk classes of water substance are modeled: vapor, non-precipitating cloud condensate, and rain, with associated mass fractions $q_{\rm v}$, $q_{\rm c}$, and $q_{\rm r}$, respectively. Microphysical transformations between vapor and cloud condensate are handled by a saturation adjustment routine, which prevents relative humidity from exceeding 100% (i.e., abundant cloud condensation nuclei are assumed to be present) and evaporates cloud condensate in subsaturated air. Conversion of non-precipitating cloud condensate to rain is modeled as autoconversion according to

$$a = -q_{\rm c}/\tau_{\rm a}, \tag{1}$$

where a ($\rm s^{-1}$) is the sink of cloud condensate from autoconversion and $\tau_{\rm a}$ (s) is an autoconversion timescale. We set $\tau_{\rm a} = 25$ minutes, which was found to produce a similar mean cloud fraction profile as the Lin-Lord-Krueger microphysics scheme. We do not set

an autoconversion threshold for q_c. Rain is given a fixed freefall speed of 8 m/s. When rain falls through subsaturated air, it is allowed to evaporate according to

$$e = (q_v^* - q_v)/\tau_r, \tag{2}$$

where e (s^{-1}) is the rate of rain evaporation, q_v^* is the saturation specific humidity, and τ_r (s) is a rain-evaporation timescale. We set $\tau_r = 50$ hours, which was found to produce a tropospheric relative humidity profile similar to that of the Lin-Lord-Krueger scheme.

By default, DAM parameterizes radiative transfer with RRTM (Clough et al., 2005; Iacono et al., 2008). However, to facilitate the investigation of spectrally-tuned solar radiation management, we instead coupled DAM to a brute-force (i.e., wavenumber-by-wavenumber) clear-sky radiation scheme. Our longwave calculations covered the wavenumber range from 0–3000 cm^{-1}, while our shortwave calculations covered 0–50000 cm^{-1}. The spectral resolution for both channels was 0.1 cm^{-1}. While this spectral resolution does not resolve the cores of lines at low (stratospheric) pressures, sensitivity tests showed that further increases in resolution yielded negligible changes to the radiative fluxes, as also found by Wordsworth et al. (2017). At each wavenumber, the monochromatic radiative transfer equation was solved using the approach described in (Schaefer et al., 2016), which uses the layer optical depth weighting scheme of (Clough et al., 1992) to ensure accurate model behavior in strongly-absorbing portions of the spectrum. To compute radiative fluxes, we used the two-stream approximation with first-moment Gaussian quadrature (Clough et al., 1992).

DAM's brute-force radiation scheme uses lookup tables of absorption coefficients on a pressure-temperature grid that covers the range of atmospheric conditions encountered in the model evolution, and interpolates to the current horizontal-mean atmospheric state at each vertical model level. Our pressure-temperature grid had a total of 20 pressure levels, with 10 levels spaced linearly in pressure between 1020 mb and 100 mb, and 10 levels spaced logarithmically between 100 mb and 0.5 mb. On each pressure level, absorption coefficients were evaluated at a set of 16 temperatures (spaced 5 K apart) that bracket the conditions encountered in the model evolution. This pressure-temperature grid is shown in Figure S1, along with mean temperature profiles from the CTRL and $4\times CO_2$ simulations. To generate the absorption-coefficient lookup tables for H_2O and CO_2 from the HITRAN2016 database (Gordon et al., 2017), we used the RFM, a publicly available line-by-line model (Dudhia, 2017). H_2O continuum absorption was modeled with version 3.2 of the MT-CKD code (Mlawer et al., 2012), also publicly available.

For shortwave radiation, we modeled gaseous absorption only, which is appropriate for clear skies at wavelengths where Rayleigh scattering is not important. In reality, Rayleigh scattering in clear skies enhances the planetary albedo, but this process is important at significantly shorter wavelengths than the near-infrared wavelengths that are the focus of spectral SRM. Therefore, the inclusion of Rayleigh scattering would introduce a small offset in the relationship between insolation and equilibrated surface temperature in our model, but would otherwise have a minimal effect on our results regarding spectral SRM.

To validate our brute-force radiation scheme, we compared its radiative fluxes and heating rates to those calculated by RRTM for a set of idealized atmospheric soundings

(Figure S2). We find quite good agreement, with differences in radiative heating rates generally smaller than 0.15 (0.1) K/day for LW (SW) radiation. We also evaluate the dependence of OLR on changing surface temperature, tropospheric relative humidity, and CO_2 concentration and find excellent agreement between RRTM and our scheme (Figure S3); although there is an offset of $\simeq 3$ W/m^2 between RRTM and our scheme for all conditions we tested, since this offset is constant in magnitude, we can infer that the radiative forcings and clear-sky feedbacks calculated by our radiation scheme match those of RRTM. Given the idealized nature of other aspects of the model framework, we consider the level of accuracy in the radiative transfer component shown in Figures S2 and S3 to be sufficient.

References

Clough, S. A., Iacono, M. J., & Moncet, J.-l. (1992). Line-by-line calculations of atmospheric fluxes and cooling rates: Application to water vapor. *Journal of Geophysical Research*, *97*(D14), 15761.

Clough, S. A., Shephard, M. W., Mlawer, E. J., Delamere, J. S., Iacono, M. J., Cady-Pereira, K., ... Brown, P. D. (2005). Atmospheric radiative transfer modeling: A summary of the AER codes. *Journal of Quantitative Spectroscopy and Radiative Transfer*, *91*(2), 233–244. doi: 10.1016/j.jqsrt.2004.05.058

Dudhia, A. (2017). The Reference Forward Model (RFM). *Journal of Quantitative Spectroscopy and Radiative Transfer*, *186*, 243–253. doi: 10.1016/j.jqsrt.2016.06.018

Gordon, I. E., Rothman, L. S., Hill, C., Kochanov, R. V., Tan, Y., Bernath, P. F., ... Zak, E. J. (2017). The HITRAN2016 molecular spectroscopic database. *Journal*

of Quantitative Spectroscopy & Radiative Transfer, *203*, 3–69. doi: 10.1016/j.jqsrt .2017.06.038

Iacono, M. J., Delamere, J. S., Mlawer, E. J., Shephard, M. W., Clough, S. A., & Collins, W. D. (2008). Radiative forcing by long-lived greenhouse gases: Calculations with the AER radiative transfer models. *Journal of Geophysical Research Atmospheres*, *113*(13), 2–9. doi: 10.1029/2008JD009944

Krueger, S. K., Fu, Q., Liou, K. N., & Chin, H.-N. S. (1995, mar). Improvements of an Ice-Phase Microphysics Parameterization for Use in Numerical Simulations of Tropical Convection. *Journal of Applied Meteorology*, *34*, 281–287.

Lin, Y.-L., Farley, R. D., & Orville, H. D. (1983). *Bulk Parameterization of the Snow Field in a Cloud Model* (Vol. 22) (No. 6).

Lord, S. J., Willoughby, H. E., & Piotrowicz, J. M. (1984, oct). Role of a Parameterized Ice-Phase Microphysics in an Axisymmetric, Nonhydrostatic Tropical Cyclone Model. *Journal of the Atmospheric Sciences*, *41*(19), 2836–2848.

Margolin, L. G., Rider, W. J., & Grinstein, F. F. (2006, jan). Modeling turbulent flow with implicit LES. *Journal of Turbulence*, *7*, N15.

Mlawer, E. J., Payne, V. H., Moncet, J.-L., Delamere, J. S., Alvarado, M. J., & Tobin, D. C. (2012). Development and recent evaluation of the MT_CKD model of continuum absorption. *Philosophical Transactions of the Royal Society A: Mathematical, Physical and Engineering Sciences*, *370*(1968), 2520–2556.

Romps, D. M. (2008). The Dry-Entropy Budget of a Moist Atmosphere. *Journal of the Atmospheric Sciences*, *65*(12), 3779–3799.

Schaefer, L., Wordsworth, R. D., Berta-Thompson, Z., & Sasselov, D. (2016). Predictions of the atmospheric composition of GJ 1132b. *The Astrophysical Journal*, *829*(2), 63. doi: 10.3847/0004-637x/829/2/63

Seeley, J. T., Jeevanjee, N., & Romps, D. M. (2019). FAT or FiTT: Are anvil clouds or the tropopause temperature-invariant? *Geophysical Research Letters*, *46*(3), 1842–1850.

Wordsworth, R., Kalugina, Y., Lokshtanov, S., Vigasin, A., Ehlmann, B., Head, J., ... Wang, H. (2017). Transient reducing greenhouse warming on early Mars. *Geophysical Research Letters*, 1–7. doi: 10.1002/2016GL071766

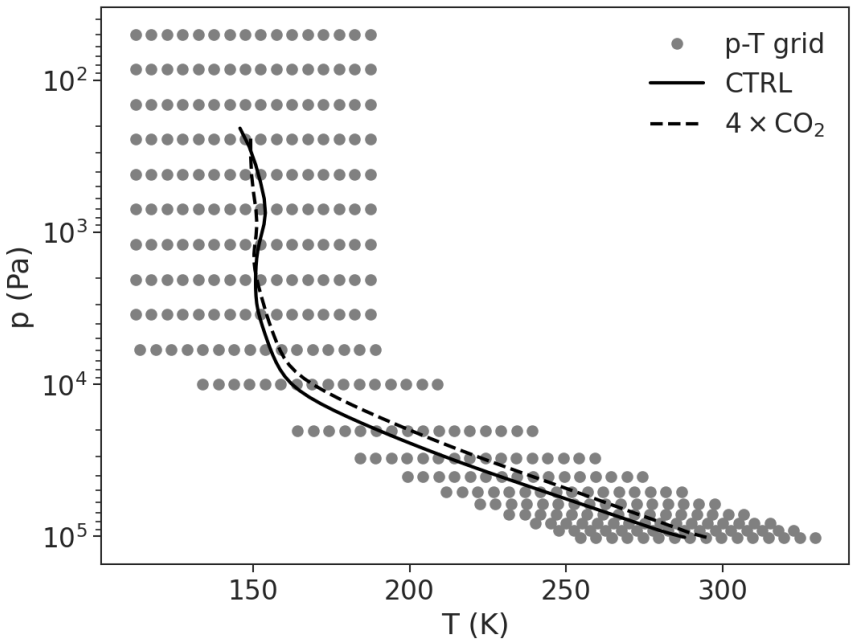

Figure S1. The pressure-temperature grid on which lookup tables of absorption coefficients for CO_2 and H_2O were generated for use in the radiative transfer calculations.

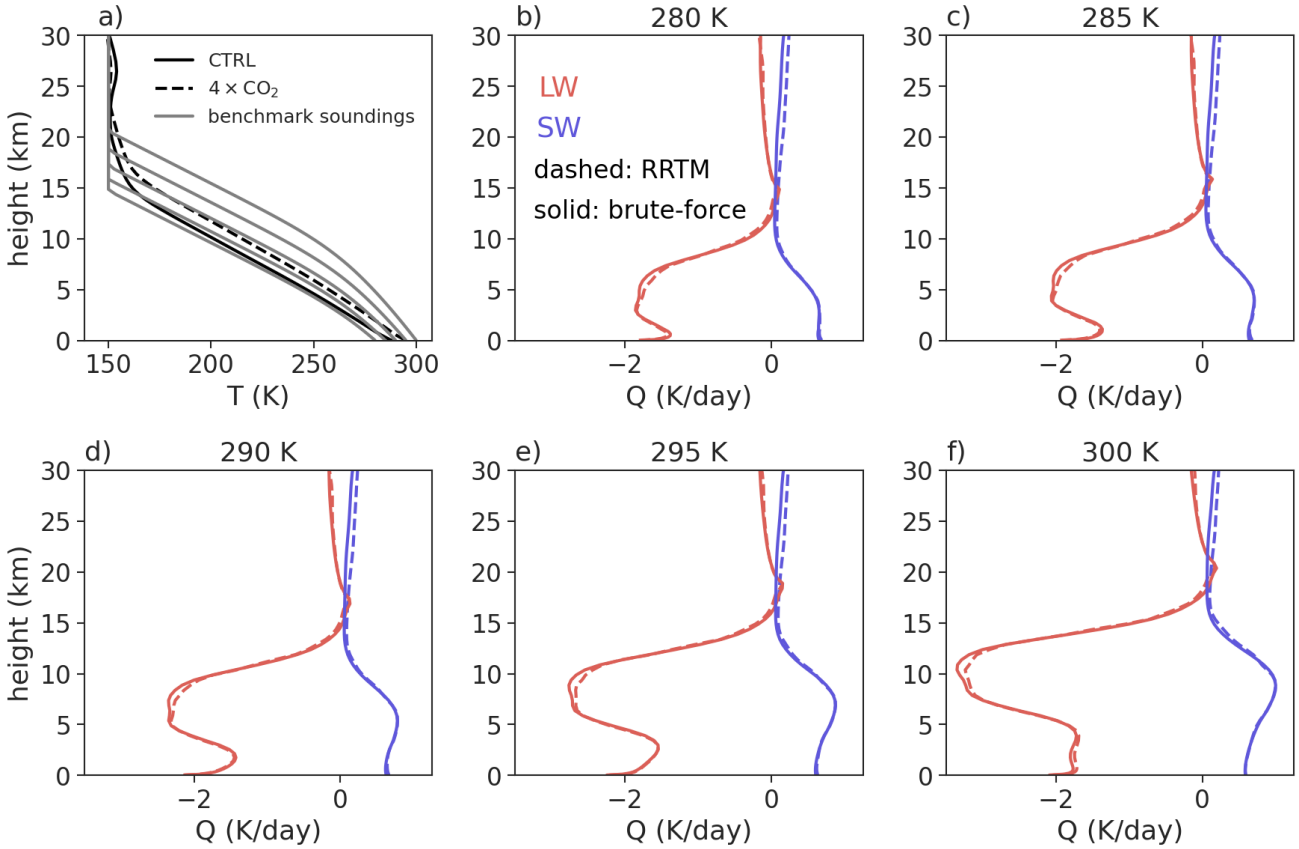

Figure S2. (a) The benchmark soundings (gray), with surface temperatures ranging from 280–300 K in 5-K increments and moist-adiabatic tropospheres. The mean temperature profiles from the CTRL and $4\times CO_2$ simulation are also plotted. (b–f) Vertical profiles of LW (red) and SW (blue) radiative heating rates for the benchmark soundings plotted in (a), as computed by RRTM (dashed) and by our brute-force radiation scheme (solid).

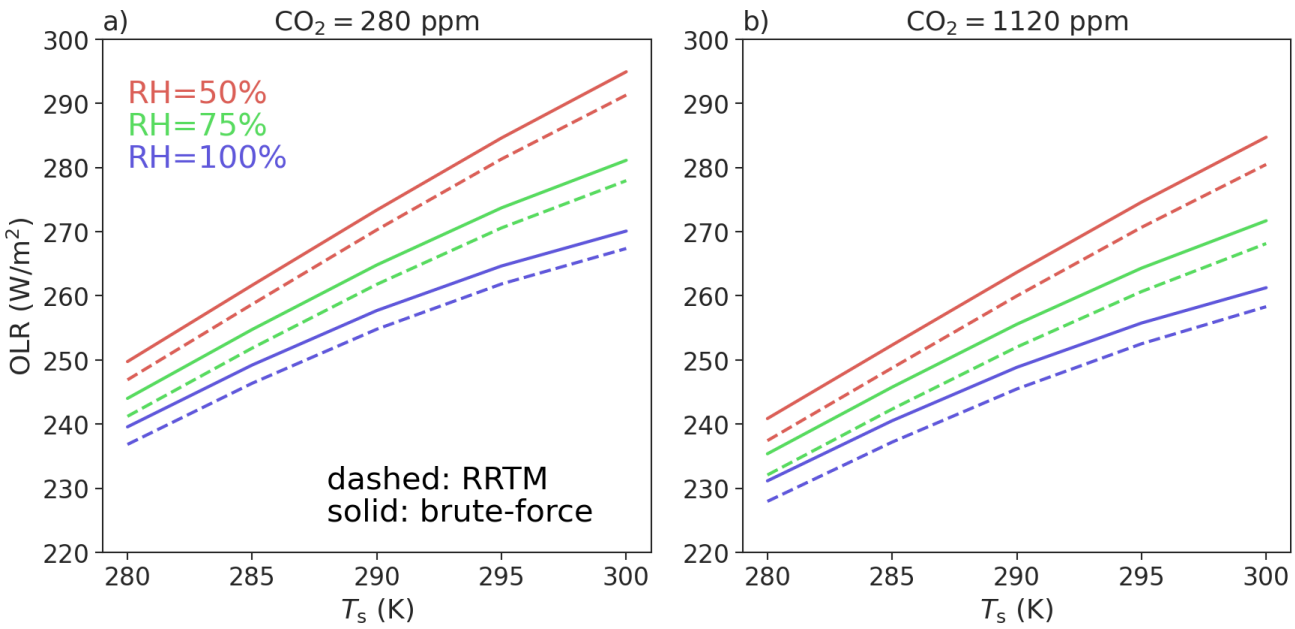

Figure S3. The dependence of OLR on surface temperature and tropospheric relative humidity, as calculated by RRTM (dashed) and by our brute-force radiation scheme (solid). Panels (a) and (b) show calculations with 280 ppm and 1120 ppm of CO_2, respectively.